A COMPARATIVE STUDY BETWEEN WIND-TUNNEL EXPERIMENTS AND RANS SIMULATIONS OF MODERN SQUARE HEADED MAIN SAILS

A B G Quérard, University of Southampton, UK P A Wilson, University of Southampton, UK

SUMMARY

A commercial code (ANSYS CFX10) which is based upon Reynolds Average Navier Stokes, is used here to compare with wind-tunnel experiments of a modern ORMA60' rig in an upwind condition. Two mainsails of different tip chord length and a head sail are tested. The flying shapes are acquired by a digital camera to feed the numerical model with the same geometry has used in the experiments. The results of the study underline the need for an extreme accuracy in the acquisition of the flying shapes. It is also noted that modelling the hull in addition to the mast and sails improve the prediction significantly. Presence of a hull tends to tangle the tip vortices generated by the sails' foot and affect the flow up to the middle of the mast, thereby increasing both lift and drag. The effects of scaling are discussed.

NOMENCLATURE

$$C_D = \frac{D}{\frac{1}{2}\rho S U_0^2}$$

$$C_I = \frac{L}{\frac{1}{2}\rho S U_0^2}$$

$$C_{mean} : \text{ mean chord length, m}$$

$$Cp = \frac{P - P_0}{\frac{1}{2}\rho U_0^2}$$

$$P : \text{ Local pressure, Pa}$$

$$P_0 : \text{ Static pressure, Pa}$$

$$Rn = \frac{U_0 c_{mean}}{v} \text{ Reynolds Number}$$

$$S : \text{ Lateral planform area, m}^2$$

$$U_0 : \text{ Axial free-stream velocity, m s}^{-1}$$

$$u^* : \text{ Friction velocity at nearest wall, m s}^{-1}$$

$$y : \text{ Distance to nearest wall, m}$$

$$y^+ = \frac{u^* y}{v}$$

$$\rho : \text{ Air density, kg, m}^{-3}$$

$$v : \text{ Kinematic fluid viscosity of air, m}^2 \text{ s}^{-1}$$

$$\tau : \text{ Stress Tensor}$$

INTRODUCTION

The design of racing yacht sails follows two main objectives: tending towards an optimal shape and then maintaining this shape under aerodynamic loading. Traditionally, wind-tunnels have been used for these purposes. In more recent times potential flow analysis has enabled estimations of drive force. The first numerical method for calculating lift and induced drag of sails was performed in 1968 by Milgram [1], [2]. The method involved the representation of the sails by vortex lattices and flat wakes. This was followed in 1989, Greeley *et al.* [3] who proposed a significant improvement to the previous method by solving iteratively the problem with the vortex wakes of the sails

convected along the streamlines at each timestep. A further step was made in 1996 by Ramsey [4], by including the aerodynamics of the above-water portion of the hull. To do so, the sails were represented using a similar approach to Greeley *et al* while the hull was represented by sources panels. Nowadays, inviscid methods are still being used for sail shape optimization in close-hauled conditions.

Since potential flow restricts the fluid to be inviscid and irrotational, this often leads to poor estimates of forces and moments on the sails when vortices or detached flows develop. On the other hand, the trend in modern racing yachts is to have sails with large square heads, as seen for example on many multihulls, and in the particular classes IACC or Open60. Linear distribution of twist along the span is a key setting, but to do so, the loading distribution on the square head has to be predicted so that reinforcement can be positioned accordingly. Unfortunately, large tip vortices govern the flow on this part of the sail, increasing the inaccuracy of flow predictions obtained using potential flow analysis.

In the mean time, Computational Fluid Dynamics (CFD) tools needed to incorporate viscous effects into design trade-off studies have developed sufficiently to be used within design cycle turn-around times. Current techniques are known as Reynolds Averaged Navier Stokes (RANS) solvers, and have seen their first practical application to upwind and downwind sail design during the 30th America's Cup. Since then, several applications of RANS have been made to the study of sails. In 2D, an example is found in the work of Doyle et al [5], who investigated the sail interactions of the Maltese Falcon, a three masts modern clipper. More recently, Chapin et al [6] combined wind-tunnel experiments with 3D RANS simulations to study the π -sail configuration of the Hydraplaneur, a catamaran designed for offshore speed records with a mast on each hull.

The present work aims to develop a methodology to study modern square head rigs in close-hauled conditions, by combining wind-tunnel experiments with 3D RANS simulations.

2. EXPERIMENTAL SET-UP

The wind-tunnel experiments took place in the low speed section of the 7 by 5 wind-tunnel of the University of Southampton. The slow speed working section has dimensions of 4.6m x 3.7m, this wind-tunnel is fitted with a six component dynamometer mounted on a turntable, dedicated to sailing yacht testing. Flow circulation underneath the hull is prevented by a water tank filled to the waterline level of the model. Wind speed was kept at 4.1m s⁻¹during all tests.

2.1 THE SAIL RIGS

The sails tested were 1:15 scale models of the Ocean Racing Multihull Association (ORMA) 60' trimarans, mounted on a One Metre class monohull with a circular section mast of diameter 0.01m. The hull was set at 25° to the wind and the sails trimmed to maximize driving force. The process of determining the maximum drive force from the settings of the sails was via the live data, being displayed and stored on the data acquisition system, directly measured from the dynamometer. The tell tales that were fitted to the main and jib sails were also used to aid this process. During testing it is apparent at maximum drive force that the top part of the sail was fluctuating in a minor manner. This indicated the presence of a vortex separation zone from the head of teh sail. This was of course to be expected. The particularities of the One Metre's rig led to a gap of 0.06m between the deck and the foot of the sails. The tests were performed with no heel, since the ORMA 60' are allowed to cant the mast laterally to maintain a vertical mast.

One jib and two mainsails were tested, as represented in Figure 1. The two mainsails, which will be denoted as *Small Main* and *Large Main* for ease of understanding, differed only with the chord length of the square head. The chord length, at model, at the square head: 0.16m for the *Small Main* and 0.29m for the *Large Main*. With a mean chord for the whole rig of 0.70m and a wind speed of 4.15m.s⁻¹, the Reynolds number is in the region of 180 000. Lateral planform areas of the various components are given in table 1.

2.2 GEOMETRY AQUISITION

A comparison between wind-tunnel measurements and numerical predictions can only be valid if the geometries used for CFD are identical to those in the wind-tunnel. It has thus been necessary to acquire the flying shape of the sails for the various wind-tunnel tests. To do so, two views were taken from a digital camera: one from the top and one from the rear, as seen in Figures 2 and 3. The freeware *Accumeasure* was then used to scan the geometries from the pictures, using a method similar to the one used by Couser and Deane [7], where Bezier

curves are fitted to the various camber stripes. In *Accumeasure*, these curves are fitted manually and their parameters used in the software *ANSYS ICEM 10.0* to generate the sails' surfaces and generate the mesh.

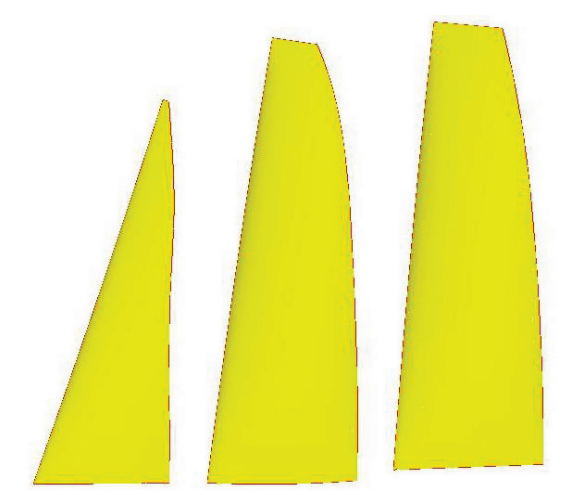


Figure 1: Side view of the jib and mainsails tested

	Lateral planform areas
Hull	0.3026m^2
Jib	0.4116m ²
Large Main	0.7355m ²
Small Main	0.6599m ²
Mast	$0.0578m^2$

Table 1: Lateral planform areas of the hull, mast and sails





Figure 2: Top view of the picture and digitalized shape

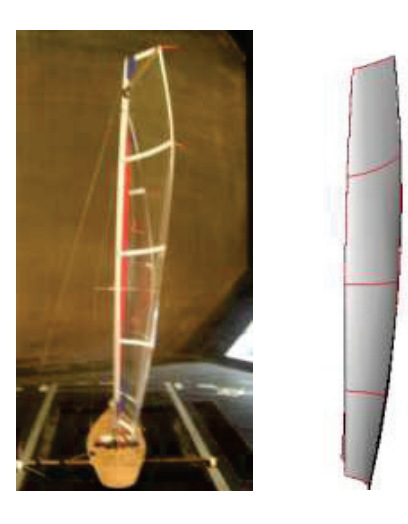


Figure 3: Aft view of the picture and digitalized shape

3. THE CFD MODEL

3.1 MATHEMATICAL THEORY

The flow solver ANSYS CFX 10.0 uses a finite volume formulation of the Reynolds Average Navier Stokes equations to model fluid flow. In Cartesian coordinates, the continuity and momentum equations written in tensor form become:

$$\frac{\partial u_i}{\partial x_i} = 0$$

$$\rho \left(\frac{\partial u_i}{\partial t} + u_j \frac{\partial u_i}{\partial x_j} \right) = -\frac{\partial P}{\partial x_i} + \frac{\partial \tau}{\partial x_j} - \frac{\partial (\rho \overline{u'_i u'_j})}{\partial x_j}$$

 τ is the molecular stress tensor:

$$\tau = \tau_{ij} = \mu \left(\frac{\partial u_i}{\partial x_j} + \frac{\partial u_j}{\partial x_i} \right)$$

And, $-\rho \overline{u'_i u'_j}$ is the so called Reynolds stress tensor, P the mean pressure, u_i are the mean velocity vector components, u' the fluctuating velocity vector, ρ the density of the fluid and μ the dynamic viscosity.

Turbulence models are required to close the RANS equations by providing models for the computation of the Reynolds stresses. One proposal suggests that turbulence consists of small eddies which are continuously forming and dissipating, and in which the Reynolds stresses are assumed to be proportional to mean velocity gradients. This assumption is the basis of the so-called eddy viscosity models. The turbulence model used here, the Shear Stress Transport (SST) model developed in 1994 by Menter [8], follows this assumption. The SST model accounts for the transport of the turbulent shear stress and gives highly accurate predictions of the onset and the amount of flow separation under adverse pressure gradients, as noted by Collie *et al* [9] in their review of turbulence models for sail flow simulations.

3.2 NUMERICAL MODELLING

The CFD calculations were all performed using *ANSYS CFX10* with two partitions on a Dual 2.2 GHz 64 bit Opteron with 4 GB RAM. Typical CPU time was 15h for mesh size of 2,418,871 cells.

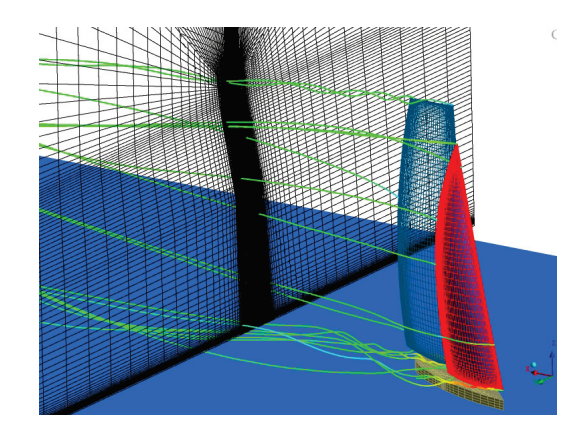
3.2 (a) Domain size and mesh

The domain size encompassed the wind-tunnel's working section: width = 4.6m, height = 3.7m, depth = 11m.

A study of the actual mesh density and size was made and after several iterations of these parameters the following was considered accurate enough in terms of the repeatability of CFD results and also the smallness of the v^+ parameter.

The 3D structured mesh used to model the wind-tunnel's walls, jib, main and mast without hull was made of 2,418,871 hexahedrons distributed as follows:

- Spanwise: 60 nodes for the jib and 80 for the main
- Chord wise: 50 nodes for the jib and 45 for the main
- Slot between the sails: 25 nodes
- Wake (longitudinally): 50 nodes
- Gap between sails' foot and deck: 15 nodes
- (1)As seen from figure 4, the nodes were distributed hyperbolically to allow for refinement at the leading and trailing edges, foot and head of the sails, in the direction (2) normal to the sails (with $y^+=O(10)$) and in the wake. An
- adaptative mesh refinement scheme was developed to track the wake according to the maximum axial velocity loss.
- The mesh of the hull was realized independently and (3) joined to the one used for the rig, using a domain interface, as proposed by Miyata and Lee [10]. 40,000 hexahedral cells were used to mesh the sub-domain containing the hull. The hull was situated 0.06m below the sails' foot, as in the experiments. For the simulations without hull, the bottom of the domain (floor) was positioned according to the deck level to ensure a similar gap below the sails.



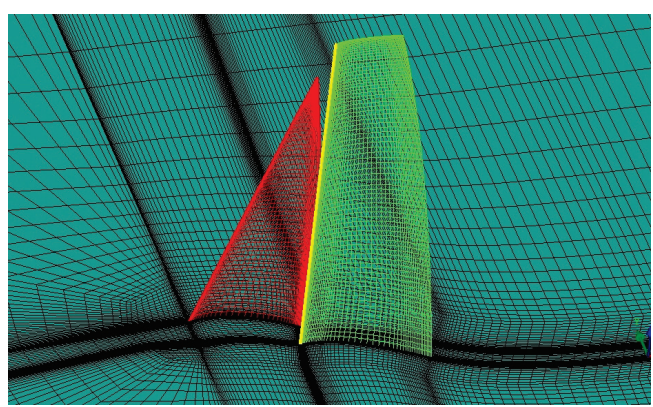


Figure 4: Views of the mesh with, and without hull

3.2 (b) Boundary conditions

A no-slip wall boundary condition was assigned to the sails, mast, floor and, whenever applicable, to the hull. The remaining tunnel's walls (sides and roof) were modelled as free-slip walls to save on computing time. The inlet was assigned a uniform velocity profile with turbulence level similar to the one recorded in the wind-tunnel: turbulence intensity of 0.2% and eddy length scale of 0.4m. A zero static pressure condition was imposed at the outlet.

3.2 (c) Numerical scheme

Each simulation was performed using a second order advection scheme and a convergence criteria of RMS(Residuals)<10⁻⁷ and to re-iterate the turbulence was modelled using the Shear Stress Transport (SST) turbulence model.

3.3 FORCE CALCULATION

It is common practice when testing sails in wind-tunnels to subtract the contributions of the hull and mast to the measured force. This is sometimes termed windage corrections. For consistency, such an approach was also taken with CFD; thus requiring two simulations: with and without sails. The forces acting on the sails were thus obtained as follows:

 $\begin{array}{l} Lift_{\ Jib+Main} = Lift_{\ Jib+Main+Mast\ (+Hull)} - Lift_{\ Mast\ (+Hull)\ alone} \\ Drag_{\ Jib+Main} = Drag_{\ Jib+Main+Mast\ (+Hull)} - Drag_{\ Mast\ (+Hull)\ alone} \end{array}$

4. RESULTS AND OBSERVATIONS

4.1 LIFT AND DRAG DIFFERENCES

The differences of drag and lift between wind-tunnel measurements and the numerical predictions were calculated using lift and drag coefficients to allow for the slight fluctuations in air density during the experiments. During each run the air temperature was also was noted. This allowed for the fluctuation of the air density during the experimental period to be dually accounted for.

$$\begin{aligned} Diff(Drag) &= \frac{Cd_{Tunnel} - Cd_{CFD}}{Cd_{Tunnel}} \\ Diff(Lift) &= \frac{Cl_{Tunnel} - Cl_{CFD}}{Cl_{Tunnel}} \end{aligned}$$

With or without modelling the hull, both drag and lift tended to be underestimated compared to the experimental results, as seen from figure 5. However, it is worth noting that the simulations of the Large Main rig led to differentials 1.7 times higher than for the Small Sail. One hypothesis to explain such a difference resides in a possible small error in the acquisition of the angle of attack from the picture. A new simulation was thus setup with the angle of attack of the whole rig increased by just 5°. Doing so, the numerical prediction led this time to negative differentials (i.e. over-prediction) of 6.9% for drag and 16.7% for lift. This would thus confirm the hypothesis that a small error of the order of 1-2 degree in the acquisition of the various angles of the sail would be large enough to cause a significant difference between the experiments and the CFD.

Having noted the influence of the accuracy in the acquisition of the angles, it is also interesting to highlight the influence of the presence of a hull in the simulation. As seen from figure 5, modelling the hull reduces the difference between the experimental force measurements and the numerical predictions. In fact, the presence of a hull in the simulation tends to increase the drag of the sails by around 6% and increases lift by around 3% for both rigs.

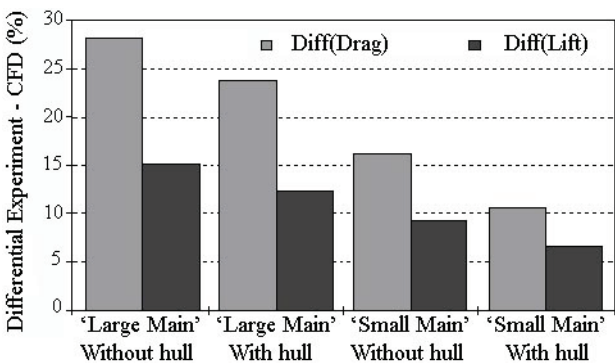


Figure 5: Differences between experimental results and CFD predictions for the two rigs, with and without modelling the hull

4.2 AXIAL VELOCITIES AT MID-SPAN

The velocity fields plotted in figure 6(a) and (c) show significant differences between the *Large Main* and the *Small Main*. In fact, on the one hand the flow on the latter seems nearly fully attached, but on the other hand, the *Large Main* exhibits a large separation bubble on its windward side, which is characteristic of a very small angle of attack, as noted by Wilkinson [11]. However, when increasing the angle of attack of the whole rig by 5°, the length of the separation bubble reduces ,as seen

in figure 6 (b). This would tend to confirm the hypothesis described in section 4.1.

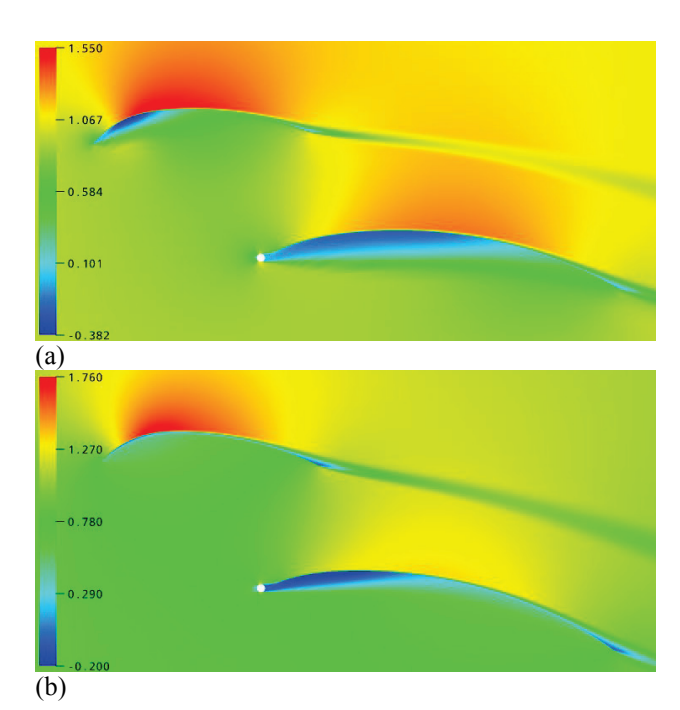
The presence of a hull in the simulation tended to increase by 2% the magnitude of the maximum axial velocity at the extrados, the outer surface, of the jib. In the same way, the hull decreased the magnitude of the backwind in the windward separation bubble of the mainsail. This would mean that, at mid-span of the mast, the presence of a hull shifts the flow so that the angle of attack of the jib is increased.

4.3 PRESSURE FIELD IN THE WAKE

The pressure distributions presented in figure 7 were obtained in a transverse plane located one boat length behind the model. It appears from figure 7(a) that in this plane, the wake consists of four distinct vortices respectively generated by:

- The foot of the mainsail
- The foot of the jib
- The head of the mainsail
- The head of the jib

When the sails and mast are solely modelled, the four vortices are clearly separated, as seen from figure 7(a). However, the presence of a hull tends to tangle the two vortices generated by the foot of each sail, as in figure 7(b). In terms of pressure magnitude, this wrapping together of the vortices in the lower part of the wake leads to a reduction by 20% in the magnitude of suction in the vortex core. Similar results were found with the *Large Main* rig.



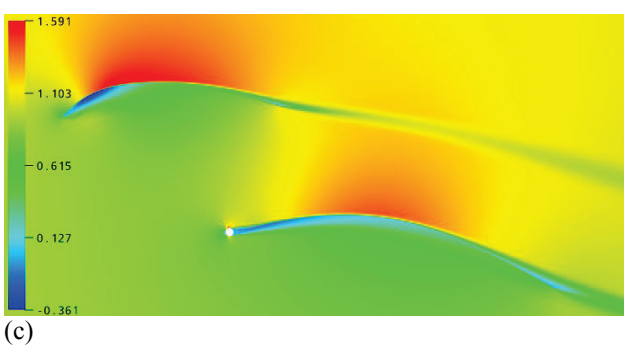
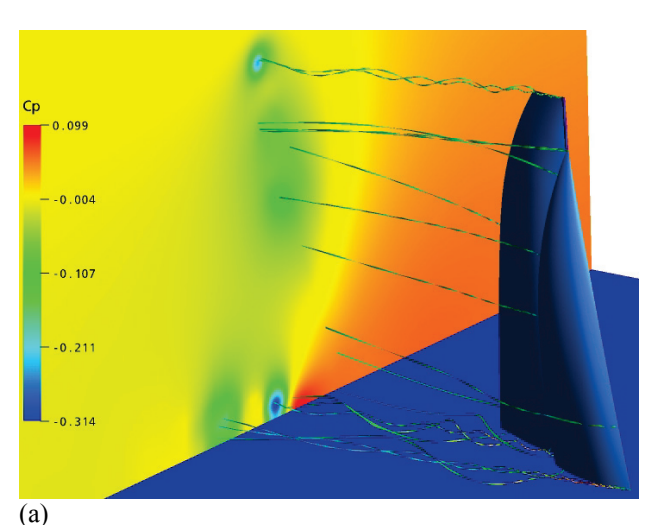


Figure 6: Velocity field of the non-dimensional axial velocity at mid-span of the mast for: (a) *Large Main*' without hull, (b) *Large Main* without hull rotated by +5°, and (c) *Small Main* without hull



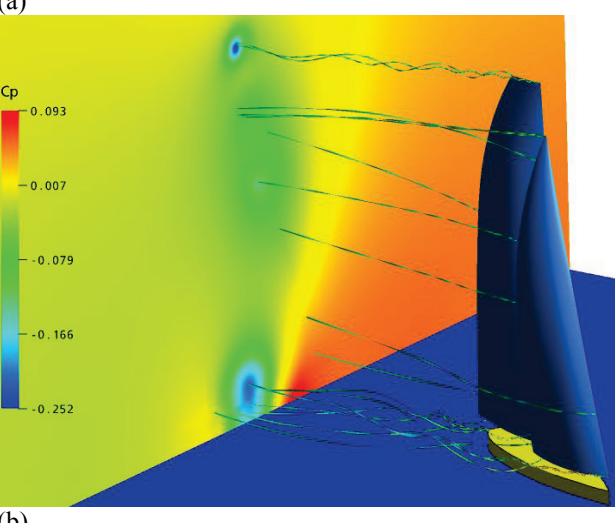


Figure 7: Streamlines and pressure distribution in the wake for: (a) 'Small Main' without hull and (b) 'Small Main' with hull

4.4 SCALING EFFECTS

The simulations so far discussed were set-up to replicate the conditions of the experiments. In particular, the scale (1:15) of the model was maintained as well as the windspeed (4.15m.s⁻¹). For this last part of the work, the *Small*

Main rig, mast and hull were scaled up to full scale while the wind-speed was given a realistic magnitude of 15 knots (7.72m.s⁻¹). The lift and drag coefficients shown in table 2 highlight that at model scale in 4.15m.s⁻¹, the lift and drag coefficients are respectively 12% and 14% lower compared to the one obtained with the full scale rig in 7.72m.s⁻¹, consequence of a Reynolds effect, namely a dependence of the aerodynamic coefficients with the Reynolds number.

	C_{L}	CD
Model (1:15) in 4.15m.s ⁻¹	1.133	0.155
Full scale rig in 15kts,(7.72 m.s ⁻¹)	1.242	0.162

Table 2 Numerical prediction of lift and drag coefficients for the *Small Main* rig with hull, at model scale and at true scale

Discrepancies were also noticed for the axial velocity fields at mid-span. In fact, on the leeward side of the jib, the peak of velocity is 2% lower at model scale in 4.15m.s⁻¹ than at full scale in 7.7m.s⁻¹.

The tip vortex generated by the head of the mainsail has also shown sensitivity to scaling: with the scaled model, the magnitude of the peak of suction in the core of the tip vortex was reduced by nearly 11% compared to the full-scale rig in 7.72m.s⁻¹. These results verify those found in the papers of the recent conference, ([13], [14,[15],[16],[17],[18]).

CONCLUSIONS

The present work aimed at developing a methodology for studying modern square head rigs in upwind conditions by combining wind-tunnel measurements with 3D RANS simulations. To do so, the flying shapes of the models were acquired from pictures taken during the wind-tunnel testing.

The CFD simulations have first highlighted the need for an extreme accuracy when acquiring the flying shapes from pictures. In particular, it was thought that a slight misalignment of the camera with respect to the model's centreline may have caused errors of the order of 1° in the actual sheeting angles, resulting in significant discrepancies between the measured and forces and the predictions.

The second point to be made is the importance of modelling the hull when simulating sail flow in upwind conditions. It has been shown that the hull does not only influence the flow in its vicinity, but has also an impact on the flow speed and direction at mid-span of the mast. Moreover, the hull has a strong influence on the tip vortices generated at the sails' foot: the presence of a hull tends to tangle these two vortices, which would be clearly separated otherwise. These tie in with wind tunnel practise. It has also been noted that this tangle-up of vortices reduces significantly the magnitude of suction in

the vortex core, hence their vorticity. Modelling the boom and spreaders could as well increase the accuracy of the simulation, but at the cost of an even more complex mesh.

The last part of the work has highlighted the importance of scaling effects. In fact, simulating a 1:15 model in a wind-tunnel or a full scale rig in a realistic breeze can lead to differences of up to 10% for the lift and drag coefficients and 11% for the suction in the upper tip vortex core. These differences are consequences of significant Reynolds effects. It would thus be preferable to test the models in stronger wind speeds. However, at this scale, exact similitude would only be achieved with wind speeds of 115m.s⁻¹, which will cause structural issues with the models.

RANS solvers have now reached a mature stage and can be used as high-end design tools to study sail flow and to perform optimization of modern rigs. Not only full scale force predictions can be achieved, but the whole flow field around the sails can be studied for a better understanding of the main flow features. However, it is still preferable to couple CFD simulations with some wind-tunnel experiments to validate the numerical model in general and the mesh in particular. Flying-shape acquisition is thus necessary, but requires very high accuracy.

6. ACKNOWLEDGEMENTS

The authors are particularly grateful to Mr. L. Gilbert and Incidences sailmakers for providing the One Metre hull, rig and sails for the model.

7. REFERENCES

- 1. MILGRAM, J.H., The aerodynamic of sails, Proc. 7th Symposium. Naval Hydrodynamics, pp.1397-1434, 1968
- 2. MILGRAM, J.H., The analytical design of yacht sails, Trans SNAME, pp.118-160, 1968
- 3. GREELEY, D.S., KIRKMAN, K.L., DREW, A.L., CROSS-WIHITER, J.H., Scientific sail shape design, Proc. 9th Chesapeake Sailing Yacht Symposium., pp. 33-80, 1989
- 4. RAMSE, W., Numerical methods for flow around lifting bodies with vortex wake rollup, PhD thesis, MIT, 1996
- 5. DOYLE, T., IACCARINO, G. and GERRITSEN, M., Sail optimization for the Maltese Falcon Clipper Yacht, Proc. HISWA 2002 conference, Amsterdam, The Netherlands, 2002
- 6. CHAPIN, V.G., NEYHOUSSER, R., JAMME, S., DULLIAND, G. and CHASSAING, P., Sailing yacht rig improvements through viscous computational fluid

- dynamics, Proc. 17th Chesapeake Sailing Yacht Symposium, 2005
- 7. COUSER, P. C., DEANE, N., Use of CFD techniques in the preliminary design of upwind sails, Proc. 14th Chesapeake Sailing Yacht Symposium, 1999
- 8. MENTER, F.R., Two-equation eddy-viscosity turbulence models for engineering applications, AIAA-Journal., Vol. 32, No 8, 1994
- 9. COLLIE, S.J., GERRITSEN, M. and JACKSON, P.S., A review of turbulence modelling for use in sail flow analysis, University of Auckland, School of Engineering Report No. 603, 2001
- 10. MIYATA, H. and LEE, Y.-W., Application of CFD simulation to the design of sails, J Marine Science and Technology. Vol. 4, pp 163-162, 1999
- 11. WILKINSON, S., Partially separated flows around 2D masts and sails, PhD Thesis, University of Southampton, 1984
- 12. LOCKE, N. J., JACKSON, P. S. and FLAY, R. J. G., Lift and Drag Distributions of Yacht Sails Using Wake Surveys. J. Fluids Eng, Vol. 118, 2, 346-351, 1996. doi:10.1115/1.2817384
- 13. HANSEN, H., JACKSON, P. S. Comparison of wind tunnel and full scale aerodynamic force measurements. HYPD, February, 2002
- 14. COIRO, D. P., NICOLOSI, F., SCHERILL, F. and MAISTO, U. Numerical and Experimental aeroelastic analysis of sails. HYPD, February, 2002
- 15. GRAF, G., and WOLF, E. CFD investigations and design integration for IACC yachts. HYPD, February, 2002.
- 16. LE PELLEY, D., EKBLOM, P. and FLAY, R. J. G. Wind tunnel testing of downwind sails. HYPD 2002
- 17. YOO, J., PARK, J. K. AHN, H. and VAN, S-K. CFD calculations on the sail-like three dimensional airfoil. HYPD, February 2006.
- 18. FLAY, R.J.G., and MILLAR, S. Experimental considerations in pressure measurements on sails: Wind tunnel and full scale. HYPD, February 2006.